photonics

MDPI

Article

Optical Absorption Coefficient and Refractive-Index Change in a Coupled Quantum Dot-Metallic Nanoparticle Structure

Sofia Evangelou

Department of Physics, School of Applied Mathematics and Natural Sciences, National Technical University of Athens, 157 80 Athens, Greece; evangelousof@gmail.com

Abstract: In the present work, we investigate the problem of the optical absorption coefficient (OAC) and refractive-index change (RIC) in a semiconductor quantum dot placed in the vicinity of a spherical metallic nanoparticle. We derive the total OAC and RIC from the density-matrix equations through different approaches, one without approximations and the other keeping only linear and third-order nonlinear terms. The derived formulae are then applied in a specific hybrid nanostructure to calculate the OAC and RIC. The results obtained from the derived formulae are used to compare cases of various interparticle distance values and applied light intensities and find that, although for specific distances and intensities the formulae may give similar results, in general, they give different results. Moreover, it becomes clear that the distance between the quantum dot and the metallic nanoparticle, in combination with the polarisation of the light field, plays a significant role in the OAC and RIC of the quantum dot. Expressly, conditional on the polarisation of the applied electric field, the OAC and RIC of the quantum dot can be either enhanced or suppressed close to the metallic nanoparticle compared to their values in the absence of the metallic nanoparticle.

Keywords: semiconductor quantum dot; metallic nanoparticle; optical absorption coefficient; refractive-index change; electromagnetic field; nonlinear optics

Citation: Evangelou, S. Optical Absorption Coefficient and Refractive-Index Change in a Coupled Quantum Dot-Metallic Nanoparticle Structure. *Photonics* **2023**, *10*, 124. https://doi.org/10.3390/photonics10020124

Received: 28 December 2022
Revised: 16 January 2023
Accepted: 17 January 2023
Published: 26 January 2023

1. Introduction

When semiconductor quantum dots are placed near plasmonic nanosystems, such as metallic nanoparticles, their optical properties change significantly. This has attracted significant attention due to the various potential applications of the coupled quantum-dot plasmonic nanostructures in several technological areas, including sensors, nanoswitches, quantum information processing and quantum communication, photocatalysis, imaging, and others [1,2]. The modification of the nonlinear optical response in quantum systems coupled with metal nanoparticles occurs due to several effects, including the altered electromagnetic field applied in the quantum under the presence of the metallic nanoparticle, the efficient exciton–plasmon coupling between the quantum dot and the metallic nanoparticle, and the change in the spontaneous decay rates in the quantum dots caused by the Purcell effect. Earlier studies designated enhanced nonlinear optical phenomena using these effects, including self-Kerr nonlinearity [3–8], cross-Kerr nonlinearity [9,10], second-harmonic generation [11,12], third-harmonic generation [13,14], nonlinear optical rectification [12,15–17], weak probe–strong pump effects [18–24], four-wave mixing [25,26], induced transparency [27–31], and enhanced refractive index without absorption [30,32].

Other nonlinear optical effects that have been extensively studied in isolated semiconductor quantum dots, see, e.g., Refs. [33–43], are the optical absorption coefficient (OAC) and the refractive index change (RIC). Recently, the two last-mentioned phenomena have been analyzed in semiconductor nanostructures, such as quantum dots, semiconductor nanoshells, and quantum wires coupled with a spherical metallic nanoparticle [44–46]. In these studies, the semiconductor nanostructures were modeled by a two-level quantum system that interacts with an electromagnetic field, while being coupled to the metallic

nanoparticle, and the used OAC and RIC were obtained by the application of perturbation theory, in which only linear terms in the first order and nonlinear terms in the third order were considered [44–46]. These works have shown that both the linear and third-order nonlinear OAC and the RIC in the semiconductor nanostructures are enhanced when the metallic nanoparticle is present. In addition, the presence of the metallic nanoparticle strongly modifies the total OAC and RIC, and the OAC may show strong bleaching effects, i.e., the formation of a dip near resonance, which, in the case of extensive increment of the light intensity, can even lead to optical transparency [44–46].

There are two main theoretical methods which are used in the study of the nonlinear optical effects in quantum dots coupled with metallic nanoparticles. The first method uses nonlinear density-matrix equations for the light–matter interaction that contain both the modification of the electric field that drives the quantum dot due to the presence of the metallic nanoparticle, as well as the exciton–plasmon coupling which leads to self-interaction effects. This is used for small metallic-nanoparticle radii [4,6,8–13,15,18,19,22–24,26–28,32]. The other main method uses linear density-matrix equations for the light–matter interaction which considers mainly the modification of the Purcell effect in the density-matrix equations and the modification of the driving electric field of the quantum dot due to scattering from the metallic nanoparticle. This is used in relatively large metallic-nanoparticle radii [3,5,12–14,16,17,20,21,25,29–31]. Here, we use the first method, the approach used in previous works [12,24], as this is the one proper for the radii of metallic nanoparticles that we study.

In the present study, we revisit the investigation of the OAC and RIC in a hybrid nanostructure which is comprised of a semiconductor quantum dot coupled to a spherical metallic nanoparticle. Initially, we extract the equations for the total OAC and RIC. To achieve that, we model the exciton in the quantum dot using a two-state quantum system that interacts with laser pulses, under the rotating-wave approximation, and take into account the contribution of the metallic nanoparticle. We use the solution of the density-matrix equations in steady state without approximations; hence, it is important to accurately consider the terms of the population decay time T_1 and the dephasing time T_2, which are not necessarily equal to each other in semiconductor quantum dots. We proceed following an alternative route, using the derived general formulae to obtain approximate forms of the OAC and RIC that, now, also include the first- and third-order terms.

These formulae are generalizations of those obtained with perturbation theory and used in Refs. [44–46]. Then, we advance by applying them to the calculation of the OAC and RIC in a specific semiconductor quantum dot–metallic nanoparticle system. We compare the results obtained for different interparticle distances as well as different incident light intensities and find that although for specific distances and light intensities both formulae give similar results, in general, they give different results, which may lead to a completely different form of the OAC and RIC. We show that, in general, only the case where the equations are obtained without approximations leads to accurate physical results for all parameters. Moreover, we see that the separation between the quantum dot and the metallic nanoparticle, along with the polarization of the applied electric field, is of vital importance for the total OAC and RIC of the quantum dot. In particular, for specific polarization values of the applied electric field, the OAC and RIC of the quantum dot can be either enhanced or suppressed close to the metallic nanoparticle, compared to their values without the metallic nanoparticle.

The article is structured as follows. In Section 2, we analytically show the derivation of the different formulae for the total OAC and RIC and analyze their main features. Next, in Section 3, we present results for the total OAC and RIC of the quantum dot near the metallic nanoparticle obtained by the two formulae and compare their properties. We also analyze the effects of the separation of the quantum dot and the metallic nanoparticle, the incident light intensity, and the applied field's polarization on the total OAC and RIC. Finally, in Section 4, we conclude our work.

2. Theory

Figure 1 presents the system under study. We consider a quantum dot placed at distance d along the z axis from a spherical metallic nanoparticle, creating a hybrid nanostructure. The surrounding environment is a dielectric with real relative dielectric constant ϵ_d. We treat the metallic nanoparticle as a spherical classical particle of radius a. Its optical properties are described by a Drude-type relative dielectric function $\epsilon_m(\omega) = 1 - \frac{\omega_p^2}{\omega^2 + i\omega\Gamma}$, where ω_p is the plasma frequency and Γ the electron relaxation rate. An electromagnetic field with electric field $E(t) = \tilde{E}_0 e^{-i\omega t} + \tilde{E}_0^* e^{i\omega t}$, where $\tilde{E}_0$ is the electric field amplitude and ω the angular frequency, is applied to the system. The electric field that interacts with the quantum dot is modified by the existence of the plasmonic nanoparticle and it is given in the quasi-static limit by $E_0 = l(\omega, d)\tilde{E}_0$ [47–49], where the modification factor reads

$$l(\omega, d) = \left[1 + g\frac{2\gamma(\omega)a^3}{(a+d)^3}\right], \tag{1}$$

with $g = 2$ for an electric field polarized along the z axis and $g = -1$ for an electric field polarized along the x axis. In addition, $\gamma(\omega) = \frac{\epsilon_m(\omega) - \epsilon_d}{\epsilon_m(\omega) + 2\epsilon_d}$.

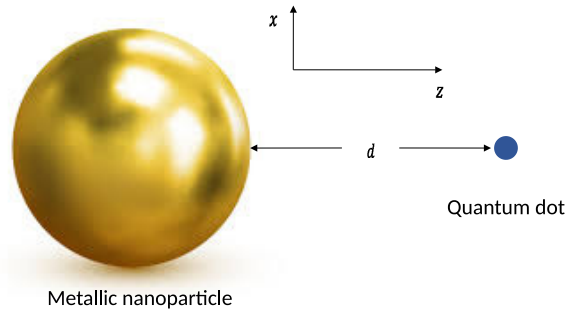

Figure 1. The schematic of the system under study. A quantum dot is placed at distance d away from the surface of a metallic nanoparticle.

The nanostructure is treated as a two-level quantum system. Therefore, the Hamiltonian that describes the interaction of the nanostructure with the electromagnetic field is

$$\hat{H} = \hbar\omega_1|1\rangle\langle 1| + \hbar\omega_2|2\rangle\langle 2| - \mu_{12}(E_0 e^{-i\omega t} + E_0^* e^{i\omega t})(|1\rangle\langle 2| + |2\rangle\langle 1|), \tag{2}$$

where $|1\rangle$ and $|2\rangle$ represent the lower and upper state, and $\hbar\omega_1$, $\hbar\omega_2$ their energies, respectively. In addition, $\mu_{12}(= \mu_{21})$ is the electric dipole matrix element (taken as real for simplicity). We note that in order to describe the electric field interacting with the quantum dot in a more precise way, we should consider both the field E_0 and the field arising by the dipole–dipole exciton–plasmon coupling, see, e.g., [6,8–10], which takes the form $E_{dd} = \frac{1}{\pi\epsilon_d}\frac{\gamma(\omega)a^3}{(a+d)^6}\mu_{12}\sigma$, with σ being the off-diagonal slowly varying element of the density matrix. Yet, for the range of the parameters of interest in this study, this field takes values which are about five to six orders of magnitude lower than $|E_0|$, and it is, therefore, omitted here.

The equations derived from the density matrix, under the rotating wave approximation, for the slowly varying elements of the density matrix are given by [50,51]

$$\dot{\sigma}(t) = \left[i(\omega - \omega_{21}) - \frac{1}{T_2}\right]\sigma(t) - i\frac{\mu_{12}E_0}{\hbar}w(t), \tag{3}$$

$$\dot{w}(t) = 2i\frac{\mu_{12}}{\hbar}[\sigma^*(t)E_0 - \sigma(t)E_0^*] - \frac{w(t)+1}{T_1}. \tag{4}$$

Here, $w(t) = \rho_{22}(t) - \rho_{11}(t)$, $\sigma(t) = \rho_{21}(t)e^{i\omega t}$, with ρ_{nm} being the density matrix element and $\omega_{21} = \omega_2 - \omega_1$.

From Equations (3) and (4), under steady-state conditions, we obtain

$$\sigma = \frac{\mu_{12}E_0}{\hbar}\frac{(\omega_0-\omega)T_2^2 + iT_2}{1+(\omega-\omega_0)^2T_2^2 + 4\frac{\mu_{12}^2|E_0|^2}{\hbar^2}T_1T_2}. \tag{5}$$

Then, the electric susceptibility of the quantum dot is given by

$$\chi = \frac{N\mu_{12}}{\varepsilon_0 E_0}\sigma = \frac{N\mu_{12}^2}{\hbar\varepsilon_0}\frac{(\omega_0-\omega)T_2^2 + iT_2}{1+(\omega-\omega_0)^2T_2^2 + 4\frac{\mu_{12}^2|E_0|^2}{\hbar^2}T_1T_2}, \tag{6}$$

where N describes electron volume density of the quantum dot.

Equation (6) is used for deriving the OAC as

$$\alpha_{tot}(\omega, I, d) = \frac{\omega}{nc}\mathrm{Im}(\chi) = \frac{\omega}{nc}\frac{N\mu_{12}^2}{\hbar\varepsilon_0}\frac{T_2}{1+(\omega-\omega_0)^2T_2^2 + 2\frac{\mu_{12}^2 I|l(\omega,d)|^2}{\hbar^2 n\varepsilon_0 c}T_1T_2}, \tag{7}$$

where n gives the refractive index of the semiconductor material. In addition, we describe the applied light-field intensity by $I = 2n\varepsilon_0 c|\tilde{E}_0|^2$. In addition, the RIC is obtained by

$$\frac{\Delta n_{tot}(\omega, I, d)}{n} = \frac{1}{2n^2}\mathrm{Re}(\chi) = \frac{N\mu_{12}^2}{2n^2\hbar\varepsilon_0}\frac{(\omega_0-\omega)T_2^2}{1+(\omega-\omega_0)^2T_2^2 + 2\frac{\mu_{12}^2 I|l(\omega,d)|^2}{\hbar^2 n\varepsilon_0 c}T_1T_2}. \tag{8}$$

We expand $\alpha_{tot}(\omega, I, d)$ and $\frac{\Delta n_{tot}(\omega,I,d)}{n}$ in a power series in terms of $k = 2\frac{\mu_{12}^2 I|l(\omega,d)|^2}{\hbar^2 n\varepsilon_0 c}T_1T_2$, and keep only terms up to k. Then, the OAC reads

$$\alpha(\omega, I, d) = \alpha^{(1)}(\omega) + \alpha^{(3)}(\omega, I, d), \tag{9}$$

where

$$\alpha^{(1)}(\omega) = \frac{\omega}{nc}\frac{N\mu_{12}^2}{\hbar\varepsilon_0}\frac{T_2}{1+(\omega-\omega_0)^2T_2^2}, \tag{10}$$

$$\alpha^{(3)}(\omega, I, d) = -\frac{2\omega N\mu_{12}^4}{\hbar^3 n^2\varepsilon_0^2 c^2}\frac{T_1T_2^2}{\left[1+(\omega-\omega_0)^2T_2^2\right]^2}I|l(\omega,d)|^2, \tag{11}$$

and the RIC is given by

$$\frac{\Delta n(\omega, I, d)}{n} = \frac{\Delta n^{(1)}(\omega)}{n} + \frac{\Delta n^{(3)}(\omega, I, d)}{n}, \tag{12}$$

where

$$\frac{\Delta n^{(1)}(\omega)}{n} = \frac{N\mu_{12}^2}{2n^2\hbar\varepsilon_0}\frac{(\omega_0-\omega)T_2^2}{1+(\omega-\omega_0)^2T_2^2}. \tag{13}$$

$$\frac{\Delta n^{(3)}(\omega, I, d)}{n} = -\frac{N\mu_{12}^4}{\hbar^3 n^3\varepsilon_0^2 c}\frac{T_1T_2^3(\omega_0-\omega)}{\left[1+(\omega-\omega_0)^2T_2^2\right]^2}I|l(\omega,d)|^2. \tag{14}$$

Here, $\alpha^{(1)}$ and $\frac{\Delta n^{(1)}}{n}$ represent the linear OAC and RIC, respectively, while $\alpha^{(3)}$ and $\frac{\Delta n^{(3)}}{n}$ give the third-order OAC and RIC, respectively. For $T_1 = T_2 = 1/\Gamma$, Equations (10), (11), (13) and (14) simply describe the widely used formulae for OAC and RIC in quantum dots that is obtained by perturbation theory [44–46]. Therefore, the present formulae are

more general given that the contribution of T_1 and T_2 in OAC and RIC, which usually take different values in semiconductor nanostructures, is clarified.

Before closing this section, we would like to point out that although the formulae for α_{tot}, α, $\frac{\Delta n_{tot}}{n}$ and $\frac{\Delta n}{n}$ have been obtained for symmetric quantum dots, i.e., without permanent dipoles, the results can be also applied as a good approximation of the study of excitons in asymmetric quantum dots with permanent dipoles near metallic nanoparticles. The general form of the density-matrix equations for the interaction of light with either an isolated asymmetric quantum dot [52] or an asymmetric quantum dot near a plasmonic nanoparticle [15], under the two-level system approach, have been obtained by Paspalakis and co-workers. These equations also have additional terms with Bessel functions, which contain in their argument the permanent dipole moments. However, these terms are only essential in the low-frequency regime and for high-incident light intensities. For excitonic transitions, which are of interest here, and for typical light intensities up to 10^{12} W/m^2, the argument of the Bessel functions are very small, so only the zeroth order Bessel function contributes in the density matrix equations, which gives value 1. Therefore, in practice, the density matrix equations reduce to those presented above and, therefore, these results may also be applied in asymmetric quantum dots.

3. Results and Discussion

In the present section, we present results for the OAC and RIC for various distances, d, between the quantum system and the plasmonic nanoparticle along the z axis and for various applied light intensities, I. We consider the excitonic transition of a GaAs/AlGaAs quantum dot with transition energy $\hbar\omega_{21} = 1.546$ eV and electric dipole-matrix element $\mu_{21} = 0.65\, e$ nm for the quantum system. In addition, $\epsilon_d = 12.5$, $T_1 = 1$ ps, $T_2 = 0.5$ ps, and $N = 5 \times 10^{22}$ m^{-3}. For the dielectric function of the metallic nanoparticle, we take values $\hbar\omega_p = 3.71$ eV and $\hbar\Gamma = 0.1855$ eV, which describe the dielectric function of gold up to 2.7 eV with high accuracy [53]. The radius of the metallic nanoparticle is taken as $a = 10$ nm.

In Figure 2a, we present results for the OAC α_{tot} as a function of the photon energy $\hbar\omega$ for applied light intensity $I = 9 \times 10^9$ W/m^2 and for different values of the distance d. The electric field is z-polarized. We find that for every distance the OAC shows a Lorentzian shape with the maximum on resonance. In addition, the OAC increases when the quantum dot comes closer to the metallic nanoparticle. In addition, the width of the OAC curves decreases for distances closer to the metallic nanoparticle. In Figure 2b, we show results for the OAC α as a function of the photon energy $\hbar\omega$ for the same parameters as in Figure 2a. The behavior is different in this case. For large interparticle distances, a double-peak shape with a strong dip in resonance is created in the OAC curve. This trend represents the so-called bleaching effect. As the quantum dot is put closer to the metallic nanoparticle, the value of the OAC increases and the OAC shape initially has a weaker double-peak shape, which eventually turns into a single peak, Lorentzian form for distance, $d = 5$ nm.

Subsequently, in Figure 3, we depict results for the RIC from $\frac{\Delta n_{tot}}{n}$ in Figure 3a and $\frac{\Delta n}{n}$ in Figure 3b as function of the photon energy $\hbar\omega$ for applied light intensity $I = 9 \times 10^9$ W/m^2 and for different values of the distance d. The electric field is z-polarized. For RIC, no matter what the separation d is, a typical dispersive shape near a single resonance is found. As the quantum system comes closer to the metallic nanoparticle, the RIC value increases and the width of the curves decreases. A similar behavior is found for short distances d in Figure 3b as well. However, the RIC curve changes its shape near resonance for larger distances. A comparison of Figures 2 and 3 reveals that the distance d affects the OAC more robustly than the RIC, i.e., for the same interparticle distance d, the OAC changes more significantly than the RIC.

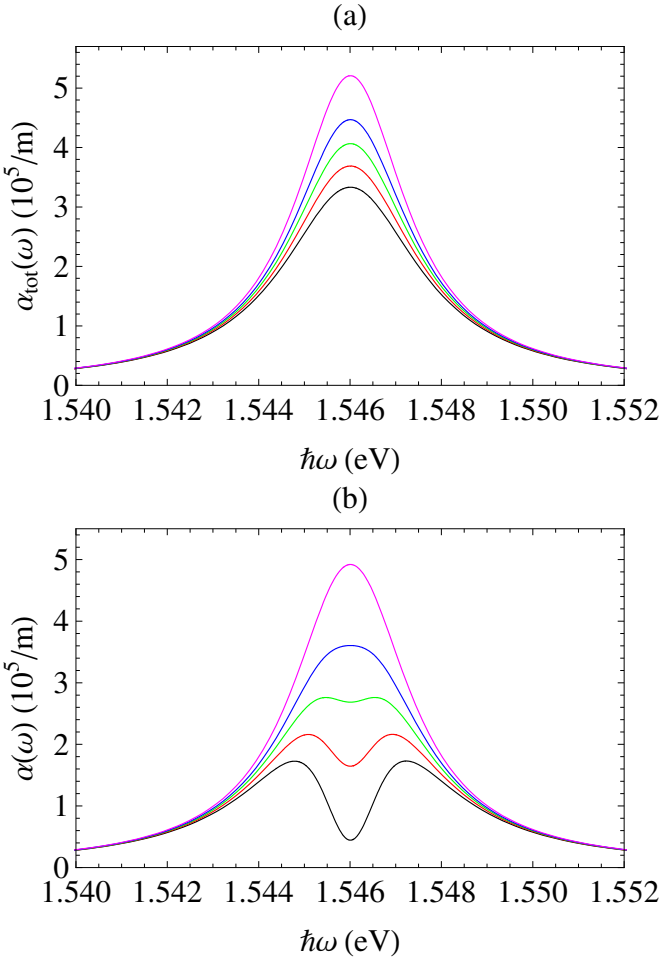

Figure 2. (Color online) The OAC $\alpha_{tot}(\omega, I, d)$ (**a**) and $\alpha(\omega, I, d)$ (**b**). The various curves are for different distances from the surface of the metallic nanoparticle: $d = 80$ nm (black curve), $d = 15$ nm (red curve), $d = 10$ nm (green curve), $d = 7.5$ nm (blue curve), and $d = 5$ nm (magenta curve). The intensity is $I = 9 \times 10^9$ W/m^2 and the field is polarized along the z axis.

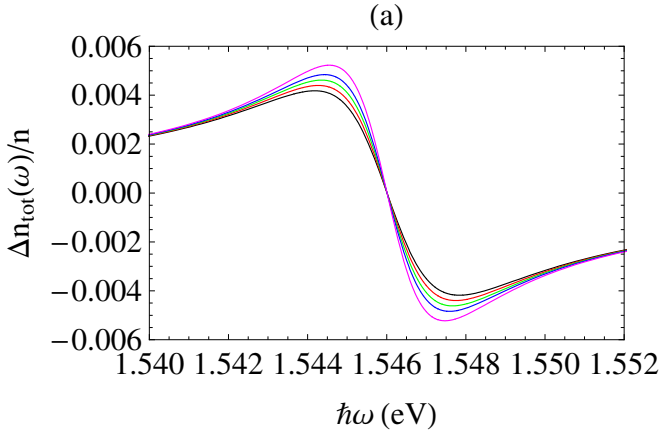

Figure 3. *Cont.*

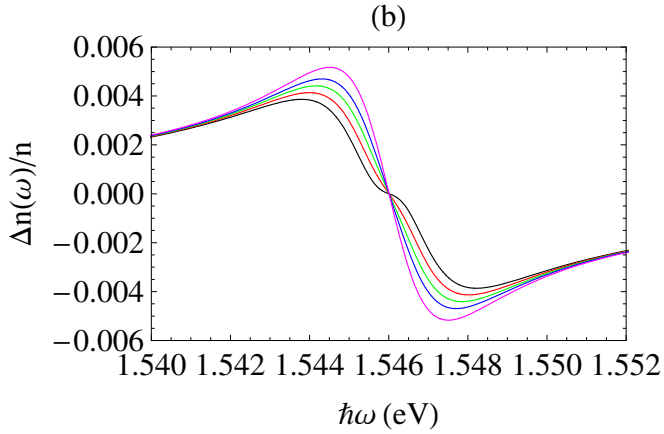

Figure 3. (Color online) The RIC $\frac{\Delta n_{tot}(\omega,I,d)}{n}$ (**a**) and $\frac{\Delta n(\omega,I,d)}{n}$ (**b**). The various curves are for different distances from the surface of the metallic nanoparticle: $d = 80$ nm (black curve), $d = 15$ nm (red curve), $d = 10$ nm (green curve), $d = 7.5$ nm (blue curve), and $d = 5$ nm (magenta curve). The intensity is $I = 9 \times 10^9$ W/m^2 and the electric field is polarized along the z axis.

In Figure 4, we show how the OAC depends on resonance, i.e., for $\omega = \omega_{21}$, from α_{tot} and α as a function of the distance d and for different light intensities I for a z-polarized electric field. We should indicate that although, when the quantum system is placed close to the metallic nanostructure, the results for OAC from the two different formulae are (almost) identical, as the distance between them increases, the results of the two formulae differentiate significantly and the OAC derived from α decreases more rapidly than the one from α_{tot}. In addition, the difference between the two curves is stronger for larger intensities. Note that for $I = 10^{10}$ W/m^2, the OAC from α becomes negative with the increase in the distance d.

Furthermore, we present results for the OAC (Figure 5) and RIC (Figure 6) for the same intensity and distances d as in Figures 2 and 3, but for the electric field polarized along the x axis. The OAC and RIC from formulae α_{tot} (Figure 5a) and $\frac{\Delta n_{tot}}{n}$ (Figure 6a), respectively, shows similar shape as with the other polarization shown in Figures 2a and 3a, i.e., Lorentzian for the OAC and typical dispersive near a single resonance for the RIC. However, in this case, the OAC and RIC values decrease as the two particles move away from each other. In addition, the width of the OAC and RIC curves increase with the decrease in distance d. The shape of the OAC and RIC from formulae α (Figure 5b) and $\frac{\Delta n}{n}$ (Figure 6b) is quite different from those presented in Figures 5a and 6a. Specifically, the OAC for large interparticle distances d has a double-peak form but it is always positive. With the decrease in the distance d, the double-peak structure becomes more pronounced and even becomes negative near resonance. As the distance d becomes shorter, the negative part of the OAC becomes stronger. The RIC also changes significantly when the two particles come closer to each other and obtains a positive slope near resonance for short distances d.

In Figure 7, we depict the dependence of the OAC on resonant frequency, i.e., for $\omega = \omega_{21}$, from α_{tot} and α as a function of the distance d and for different light intensities I for an x-polarized electric field. In this case, for all distances, the two formulae give different results and we obtain an increase in the OAC when increasing the distance between the quantum dot and the metallic nanoparticle. In addition, the difference between the two curves is larger for larger intensities. In addition, for $I = 10^{10}$ W/m^2, the OAC from α is negative for all distances.

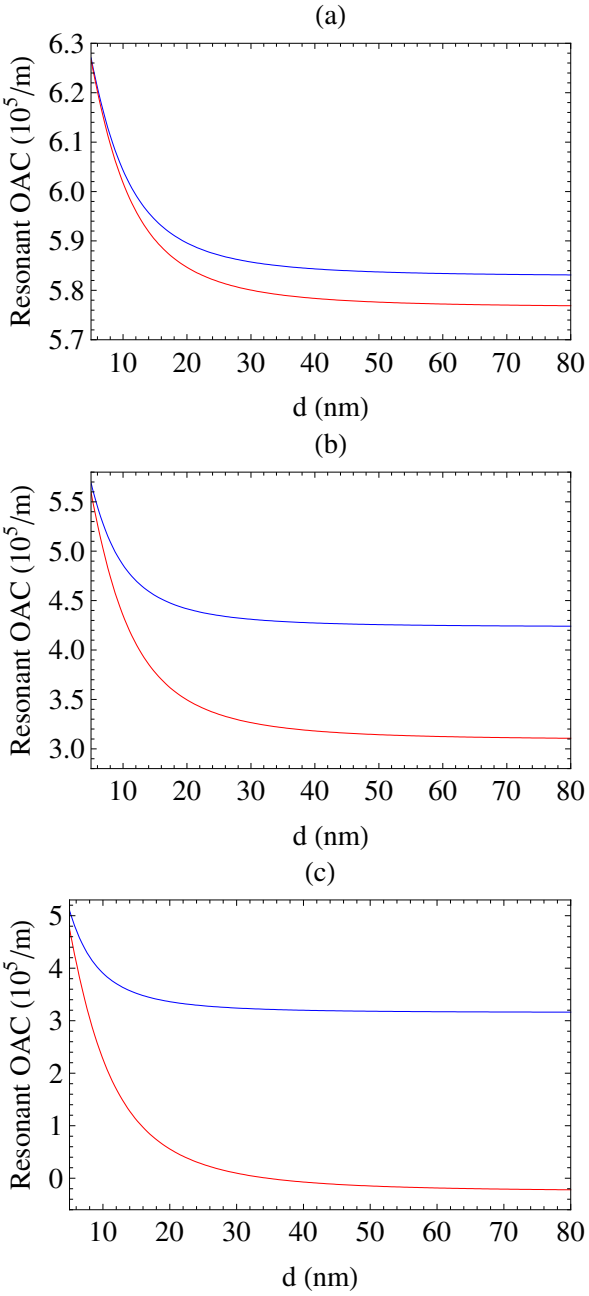

Figure 4. (Color online) The OAC on resonance, $\omega = \omega_{21}$, as a function of distance d for the electric field polarized along the z axis. The light intensities are (**a**) $I = 10^9$ W/m^2, (**b**) $I = 5 \times 10^9$ W/m^2, and (**c**) $I = 10^{10}$ W/m^2. With blue curve, we plot $\alpha_{tot}(\omega_{21}, I, d)$ and with red curve, we plot $\alpha(\omega_{21}, I, d)$.

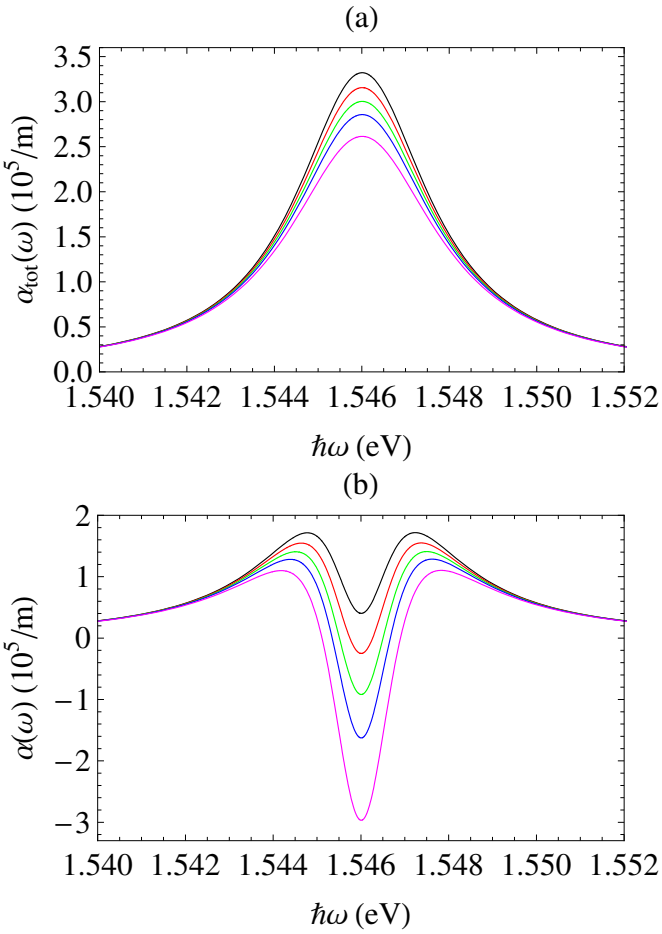

Figure 5. (Color online) The same as in Figure 2 but for the electric field polarized along the x axis.

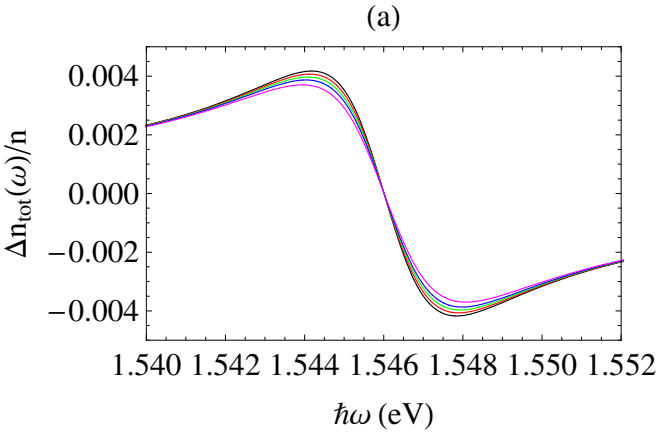

Figure 6. *Cont.*

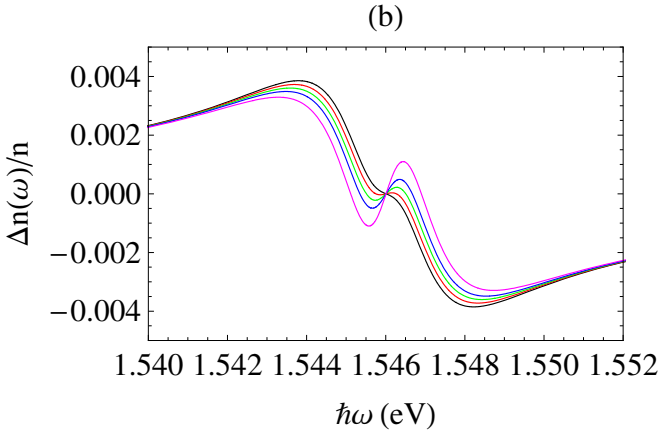

Figure 6. (Color online) The same as in Figure 3 but for the electric field polarized along the x axis.

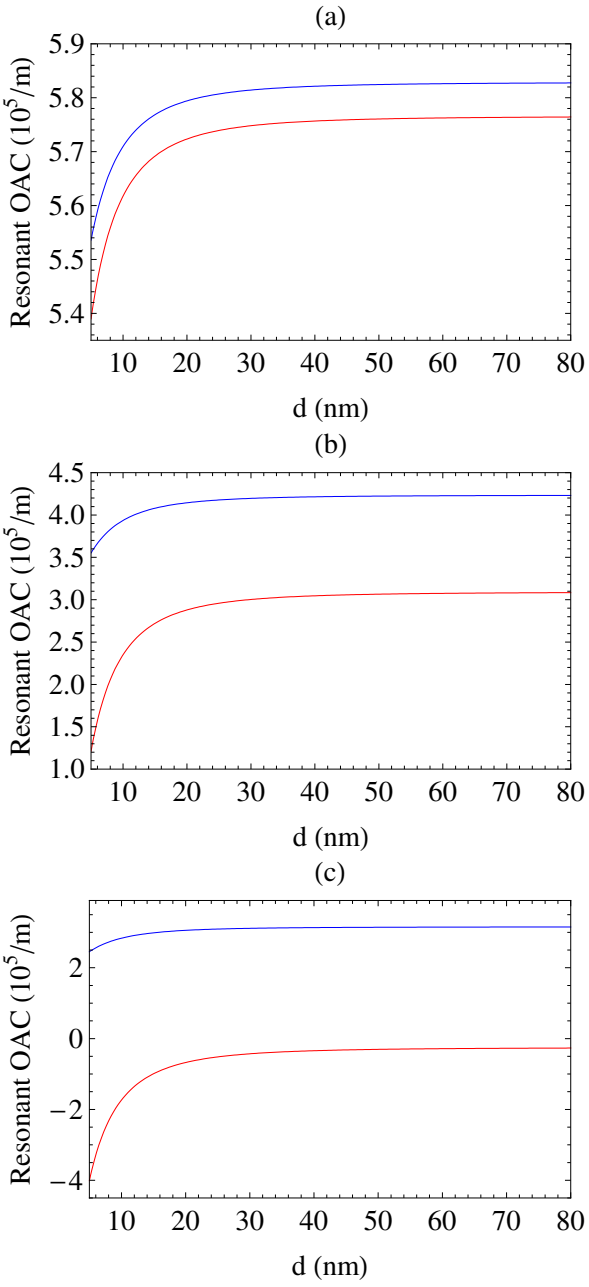

Figure 7. (Color online) The same as in Figure 5 but for the electric field polarized along the x axis.

One way to interpret the performance of the obtained results in terms of the two polarization statuses of light is to consider the value of the electric field that interacts with the quantum dot at a specific distance d. In Figure 8, we plot the absolute value of the field modification factor $l(\omega, d)$ on resonance, i.e., for $\omega = \omega_{21}$, as a function of distance for the two light polarizations. We obtain that for a z-polarized field, $|l(\omega_{21}, d)|$ decreases as the distance between the quantum dot and the metallic nanoparticle decreases, while we observe the opposite in the case of an x-polarized field. The reason for this is the interference occurring between the incident field and the scattered field from the metallic nanoparticle, i.e, destructive interference for a z-polarized field and constructive interference for an x-polarized field. Using this in Equations (7) and (8), we can justify the increment or the decrement in the OAC and RIC as a function of distance for the two different polarizations of light. The above behavior explains the results presented in Figures 2–7 regarding the change in the distance between the quantum system and the metallic nanoparticle, as larger electric fields create strong saturation, but small electric fields do not create saturation effects.

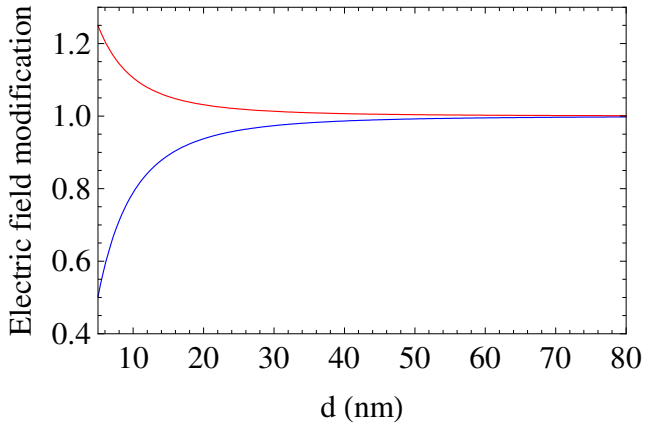

Figure 8. (Color online) The variation in the electric-field modulation term $|l(\omega_{21}, d)|$ as a function of distance d for a z-polarized electric field (blue curve) and x-polarized electric field (red curve).

Before closing, we would like to comment on the validity of the derived formulae for OAC and RIC. Formulae α_{tot} and $\frac{\Delta n_{tot}}{n}$ weer obtained without approximations regarding light intensity, besides the rotating-wave approximation. However, α and $\frac{\Delta n}{n}$ were obtained by a series expansion on incident light intensity I, keeping terms up to first order to I. We can define

$$I_{sat} = \frac{\hbar^2 n \varepsilon_0 c}{2\mu_{12}^2 T_1 T_2 |l(\omega, d)|^2}, \tag{15}$$

and we rewrite $k = \frac{I}{I_{sat}}$. It is obvious that the formulae α and $\frac{\Delta n}{n}$ are only valid in the regime in which $I \ll I_{sat}$. In the regime in which α $[\frac{\Delta n}{n}]$ deviates from α_{tot} $[\frac{\Delta n_{tot}}{n}]$, it is clear that the above condition is not fulfilled. For example, for $d = 15$ nm, $\omega = \omega_{21}$ and a z-polarized field, we take $I_{sat} = 1.2 \times 10^{10}$ W/m^2, and for a x-polarized field we take $I_{sat} = 8.66 \times 10^9$ W/m^2; therefore, for $I = 9 \times 10^9$ W/m^2, which we used in Figures 2, 3, 5 and 6, we have $I = 0.744 I_{sat}$ for a z-polarized field and $I = 1.03 I_{sat}$ for an x-polarized field. Therefore, the condition $I \ll I_{sat}$ is not fulfilled in either case. This is why α and $\frac{\Delta n}{n}$ may lead to non-physical results if they are used in a regime in which the condition $I \ll I_{sat}$ does not hold, such as, for example, the negative values of OAC shown above. This cannot happen, since in the case under study, in which no other fields are applied to the system, negative OAC values create gain and the self-amplification of the probe field; therefore, the conservation of energy is violated.

4. Conclusions

In the present study, we studied thoroughly the OAC and RIC in a semiconductor quantum dot near a spherical metallic nanoparticle. We initially derived the total OAC and RIC from the density-matrix equations under steady state without approximations and properly considered the effect of the population decay time and the dephasing time in the formulae, which may have different values, in general, in semiconductor quantum dots. We also used the derived general formulae for obtaining approximate forms of the OAC and RIC, which include the linear and third-order nonlinear terms as well. The latter formulae are generalizations of those obtained using perturbation theory, and used in Refs. [44–46]. Afterwards, we used the derived formulae to calculate the OAC and RIC in a specific case of a semiconductor quantum-dot–metallic-nanoparticle system. We used the interparticle distance as well as the electric-field intensity as parameters to compare the results obtained from the derived formulae and concluded that although for specific distances and intensities the formulae may give similar results, in general, they give different results. The correct physical behavior comes from the formulae obtained without approximations. Moreover, we found that the distance between the quantum dot and the metallic nanoparticle in combination with the polarization of the light field play a crucial role in the OAC and RIC of the quantum dot. Specifically, depending on the polarization of the applied electric field, the OAC and RIC of the quantum dot can be either enhanced or suppressed close to the metallic nanoparticle, in comparison to their values without the metallic nanoparticle. The results of this work can be used in designing nanoscale nonlinear optical devices for various technological applications.

Funding: This research is co-financed by Greece and the European Union (European Social Fund—ESF) through the Operational Programme "Human Resources Development, Education and Lifelong Learning" in the context of the project "Reinforcement of Postdoctoral Researchers—2nd Cycle" (MIS-5033021), implemented by the State Scholarships Foundation (IKY).

Institutional Review Board Statement: Not applicable.

Informed Consent Statement: Not applicable.

Data Availability Statement: Data is available upon reasonable request.

Acknowledgments: The author thanks Vassilios Yannopapas of the Physics Department of the National Technical University of Athens for useful discussions.

Conflicts of Interest: The author declares no conflict of interest.

Abbreviations

The following abbreviations are used in this manuscript:

OAC	Optical absorption coefficient
RIC	Refractive-index change

References

1. Cao, E.; Lin, W.; Sun, M.-T.; Liang, W.; Song, Y. Exciton-plasmon coupling interactions: From principle to applications. *Nanophotonics* **2017**, *7*, 145. [CrossRef]
2. Szychowski, B.; Pelton, M.; Daniel, M.-C. Preparation and properties of plasmonic-excitonic nanoparticle assemblies. *Nanophotonics* **2019**, *8*, 517. [CrossRef]
3. Yannopapas, V. Enhancement of nonlinear susceptibilities near plasmonic metamaterials. *Opt. Commun.* **2010**, *283*, 1647–1649. [CrossRef]
4. Evangelou, S.; Yannopapas, V.; Paspalakis, E. Modification of Kerr nonlinearity in a four-level quantum system near a plasmonic nanostructure. *J. Mod. Opt.* **2014**, *61*, 1458–1464. [CrossRef]
5. Ren, J.; Chen, H.; Gu, Y.; Zhao, D.-X.; Zhou, H.; Zhang, J.; Gong, Q. Plasmon-enhanced Kerr nonlinearity via subwavelength-confined anisotropic Purcell factors. *Nanotechnology* **2016**, *27*, 425205. [CrossRef]
6. Terzis, A.F.; Kosionis, S.G.; Boviatsis, J.; Paspalakis, E. Nonlinear optical susceptibilities of semiconductor quantum dot–metal nanoparticle hybrids. *J. Mod. Opt.* **2016**, *63*, 451–461. [CrossRef]

7. Evangelou, S. Modifying the linear and nonlinear optical susceptibilities of coupled quantum dot-metallic nanosphere systems with the Purcell effect. *J. Appl. Phys.* **2018**, *124*, 233103. [CrossRef]
8. Kosionis, S.G.; Paspalakis, E. Control of self-Kerr nonlinearity in a driven coupled semiconductor quantum dot–metal nanoparticle structure. *J. Phys. Chem. C* **2019**, *123*, 7308–7317. [CrossRef]
9. Lu, Z.; Zhu, K.-D. Slow light in an artificial hybrid nanocrystal complex. *J. Phys. B* **2009**, *42*, 015502. [CrossRef]
10. Li, J.-B.; Kim, N.-C.; Cheng, M.-T.; Zhou, L.; Hao, Z.-H.; Wang, Q.-Q. Optical bistability and nonlinearity of coherently coupled exciton-plasmon systems. *Opt. Express* **2012**, *20*, 1856–1861. [CrossRef] [PubMed]
11. Singh, M.R. Enhancement of the second-harmonic generation in a quantum dot–metallic nanoparticle hybrid system. *Nanotechnology* **2013**, *24*, 125701. [CrossRef]
12. Evangelou, S. Tailoring second-order nonlinear optical effects in coupled quantum dot-metallic nanosphere structures using the Purcell effect. *Microelectr. Eng.* **2019**, *215*, 111019. [CrossRef]
13. Yang, T.; Guo, K.-X. Enhancement of surface plasmon resonances on the nonlinear optical properties in an elliptical quantum dot. *J. Opt. Soc. Am. B* **2018**, *35*, 2251–2258. [CrossRef]
14. Evangelou, S.; Angelis, C.T. Using the Purcell effect for the modification of third-harmonic generation in a quantum dot near a metallic nanosphere. *Opt. Commun.* **2019**, *447*, 36–41. [CrossRef]
15. Carreno, F.; Anton, M.A.; Paspalakis, E. Nonlinear optical rectification and optical bistability in a coupled asymmetric quantum dot-metal nanoparticle hybrid. *J. Appl. Phys.* **2018**, *124*, 113107. [CrossRef]
16. Evangelou, S. Nonlinear optical rectification of a coupled semiconductor quantum dot—Metallic nanosphere system under a strong electromagnetic field. *Physica B* **2019**, *556*, 170–174. [CrossRef]
17. Domenikou, N.; Thanopulos, I.; Yannopapas, V.; Paspalakis, E. Nonlinear Optical Rectification in an Inversion-Symmetry-Broken Molecule Near a Metallic Nanoparticle. *Nanomaterials* **2022**, *12*, 1020. [CrossRef]
18. Sadeghi, S.M. Gain without inversion in hybrid quantum dot–metallic nanoparticle systems. *Nanotechnology* **2010**, *21*, 455401. [CrossRef] [PubMed]
19. Sadeghi, S.M. Ultrafast plasmonic field oscillations and optics of molecular resonances caused by coherent exciton-plasmon coupling. *Phys. Rev. A* **2013**, *88*, 013831. [CrossRef]
20. Anton, M.A.; Carreno, F.; Calderon, O.G.; Melle, S.; Cabrera, E. Radiation emission from an asymmetric quantum dot coupled to a plasmonic nanostructure. *J. Opt.* **2016**, *18*, 025001. [CrossRef]
21. Carreno, F.; Anton, M.A.; Yannopapas, V.; Paspalakis, E. Control of the absorption of a four-level quantum system near a plasmonic nanostructure. *Phys. Rev. B* **2017**, *95*, 195410. [CrossRef]
22. Kosionis, S.G.; Paspalakis, E. Pump-probe optical response of semiconductor quantum dot–metal nanoparticle hybrids. *J. Appl. Phys.* **2018**, *124*, 223104. [CrossRef]
23. Kosionis, S.G.; Paspalakis, E. Controlling the pump-probe optical response in asymmetric tunneling-controlled double quantum dot molecule—Metal nanoparticle hybrids. *Appl. Sci.* **2021**, *11*, 11714. [CrossRef]
24. Karabulut, E.Ö.; Karabulut, I. Pump-probe optical response of a semiconductor quantum dot-metallic nanosphere hybrid system. *Europ. Phys. J. Plus* **2022**, *137*, 799. [CrossRef]
25. Paspalakis, E.; Evangelou, S.; Kosionis, S.G.; Terzis, A.F. Strongly modified four-wave mixing in a coupled semiconductor quantum dot-metal nanoparticle system. *J. Appl. Phys.* **2014**, *115*, 083106. [CrossRef]
26. Singh, S.K.; Abak, M.K.; Tasgin, M.E. Enhancement of four-wave mixing via interference of multiple plasmonic conversion paths. *Phys. Rev. B* **2016**, *93*, 035410. [CrossRef]
27. Hatef, A.; Singh, M.R. Plasmonic effect on quantum coherence and interference in metallic photonic crystals doped with quantum dots. *Phys. Rev. A* **2010**, *81*, 063816. [CrossRef]
28. Hatef, A.; Sadeghi, S.M.; Singh, M.R. Plasmonic electromagnetically induced transparency in metallic nanoparticle–quantum dot hybrid systems. *Nanotechnology* **2012**, *23*, 065701. [CrossRef]
29. Evangelou, S.; Yannopapas, V.; Paspalakis, E. Transparency and slow light in a four-level quantum system near a plasmonic nanostructure. *Phys. Rev. A* **2012**, *86*, 053811. [CrossRef]
30. Paspalakis, E.; Evangelou, S.; Yannopapas, V.; Terzis, A.F. Phase-dependent optical effects in a four-level quantum system near a plasmonic nanostructure. *Phys. Rev. A* **2013**, *88*, 053832. [CrossRef]
31. Wang, L.; Gu, Y.; Chen, H.; Zhang, J.-Y.; Cui, Y.; Gerardot, B.-D.; Gong, Q.-H. Polarized linewidth-controllable double-trapping electromagnetically induced transparency spectra in a resonant plasmon nanocavity. *Sci. Rep.* **2019**, *3*, 2879. [CrossRef]
32. Wang, Z.-P.; Yu, B.-L. Plasmonic control of refractive index without absorption in metallic photonic crystals doped with quantum dots. *Plasmonics* **2019**, *13*, 567–574. [CrossRef]
33. Unlu, S.; Karabulut, I.; Safak, H. Linear and nonlinear intersubband optical absorption coefficients and refractive index changes in a quantum box with finite confining potential. *Physica E* **2006**, *33*, 319–324. [CrossRef]
34. Xie, W.-F. Nonlinear optical properties of a hydrogenic donor quantum dot. *Phys. Lett. A* **2008**, *372*, 5498–5500. [CrossRef]
35. Karabulut, I.; Safak, H.; Tomak, M. Excitonic effects on the nonlinear optical properties of small quantum dots. *J. Phys. D Appl. Phys.* **2008**, *41*, 155104. [CrossRef]
36. Sahin, M. Third-order nonlinear optical properties of a one- and two-electron spherical quantum dot with and without a hydrogenic impurity. *J. Appl. Phys.* **2009**, *106*, 063710. [CrossRef]

37. Zeng, Z.; Garoufalis, C.; Terzis, A.F.; Baskoutas, S. Linear and nonlinear optical properties of ZnO/ZnS and ZnS/ZnO core shell quantum dots: Effects of shell thickness, impurity, and dielectric environment. *J. Appl. Phys.* **2013**, *114*, 023510. [CrossRef]
38. Paspalakis, E. Comment on "From fast light to slow light in resonantly driven quantum dot systems" [Opt. Commun. 298–299 (2013) 176–179]. *Opt. Commun.* **2015**, *357*, 195–197. [CrossRef]
39. Niculescu, E.C.; Bejan, D. Nonlinear optical properties of GaAs pyramidal quantum dots. *Physica E* **2015**, *74*, 51–58. [CrossRef]
40. Bejan, D.; Niculescu, E.C. Intense laser effects on the optical properties of asymmetric GaAs double quantum dots under applied electric field. *Eur. Phys. J. B* **2016**, *89*, 138. [CrossRef]
41. Arif, S.M.; Bera, A.; Ghosh, M. Exploring the nonlinear optical properties of impurity doped quantum dots in the light of noise-binding energy interplay. *Results Phys.* **2019**, *13*, 102139. [CrossRef]
42. Baira, M.; Salem, B.; Madhar, N.A.; Ilahi, B. Linear and Nonlinear Intersubband Optical Properties of Direct Band Gap GeSn Quantum Dots. *Nanomaterials* **2019**, *9*, 124. [CrossRef]
43. Kilic, D.G.; Sakiroglu, S.; Kasapoglu, E.; Sari, H.; Sokmen, I. Impurity-modulated optical response of a disc-shaped quantum dot subjected to laser radiation. *Photon. Nanostr. Fund. Appl.* **2020**, *38*, 100748. [CrossRef]
44. Jiang, X.; Guo, K.-X.; Liu, G.; Yang, T.; Yang, Y.-L. Enhancement of surface plasmon resonances on the nonlinear optical properties in a GaAs quantum dot. *Superlatt. Microstruct.* **2017**, *105*, 56–64. [CrossRef]
45. Yang, Y.-L.; Guo, K.-X.; Yang, T.; Lia, K.; Zhai, W.-J. Enhancement of linear and nonlinear optical absorption coefficients in spherical dome semiconductor nanoshells by surface plasmon resonances. *Physica B* **2019**, *556*, 158–162. [CrossRef]
46. Su, Y.; Guo, K.-X.; Liu, G.-H.; Yang, T.; Yu, Q.-C.; Hu, M.-L.; Yang, Y.-L. Nonlinear optical properties of semiconductor double quantum wires coupled to a quantum-sized metal nanoparticle. *Opt. Lett.* **2020**, *45*, 479–482. [CrossRef]
47. Vladimirova, Y.V.; Klimov, V.V.; Pastukhov, V.M.; Zadkov, V.N. Modification of two-level-atom resonance fluorescence near a plasmonic nanostructure. *Phys. Rev. A* **2012**, *85*, 053408. [CrossRef]
48. Vladimirova, Y.V.; Zadkov, V.N. Quantum optics in nanostructures. *Nanomaterials* **2021**, *11*, 1919. [CrossRef]
49. Novotny, L.; Hecht, B. *Principles of Nano-Optics*, 2nd ed.; Cambridge University Press: Cambridge, UK, 2012; Chapter 12.
50. Boyd, R.W. *Nonlinear Optics*, 3rd ed.; Academic Press: San Diego, CA, USA, 2008; Paragraph 6.3.
51. Zeng, Z.; Paspalakis, E.; Garoufalis, C.; Terzis, A.F.; Baskoutas, S. Optical susceptibilities in singly charged ZnO colloidal quantum dots embedded in different dielectric matrices. *J. Appl. Phys.* **2013**, *113*, 054303. [CrossRef]
52. Paspalakis, E.; Boviatsis, J.; Baskoutas, S. Effects of probe field intensity in nonlinear optical processes in asymmetric semiconductor quantum dots. *J. Appl. Phys.* **2013**, *114*, 153107. [CrossRef]
53. Kosionis, S.G.; Terzis, A.F.; Yannopapas, V.; Paspalakis, E. Nonlocal effects in energy absorption of coupled quantum dot–metal nanoparticle systems. *J. Phys. Chem. C* **2012**, *116*, 23663–23670. [CrossRef]